Biophysical Journal Volume 106 January 2014 172–181

HIV gp41 Fusion Peptide Increases Membrane Ordering in a Cholesterol-Dependent Fashion

Alex L. Lai and Jack H. Freed*

Department of Chemistry and Chemical Biology, Cornell University, Ithaca, New York

ABSTRACT Fusion between viral envelopes and host cell membranes, which is mediated by special glycoproteins anchored on the viral membrane, is required for HIV viral entry and infection. The HIV gp41 fusion peptide (FP), which initiates membrane fusion, adopts either an α-helical or β-sheeted structure depending on the cholesterol concentration. We used phosphocholine spin labels on the lipid headgroup and different positions on the acyl chain to detect its perturbation on lipid bilayers containing different cholesterol concentrations by electron-spin resonance. Our findings were as follows. 1), gp41 FP affects the lipid order in the same manner as previously shown for influenza hemagglutinin FP, i.e., it has a cooperative effect versus the peptide/lipid ratio, supporting our hypothesis that membrane ordering is a common prerequisite for viral membrane fusion. 2), gp41 FP induces membrane ordering in all lipid compositions studied, whereas a nonfusion mutant FP perturbs lipid order to a significantly smaller extent. 3), In high-cholesterol-containing lipid bilayers, where gp41 FP is in the β-aggregation conformation, its effect on the lipid ordering reaches deeper into the bilayer. The different extent to which the two conformers perturb is correlated with their fusogenicity. The possible role of the two conformers in membrane fusion is discussed.

INTRODUCTION

Membrane fusion between viral envelope and host membrane is the required step during the infection of an enveloped virus, such as the human immunodeficiency (HIV) and influenza viruses. Blocking membrane fusion can lead to the development of new antiviral drugs. The viral membrane fusion system also serves as a model for biological membrane fusion systems, because it is relatively simple. Compared to a much more complicated system, such as a synaptic vesicle membrane fusion system (1–3), which involves several proteins, only one glycoprotein is involved in the viral membrane fusion process, though multiple copies of this protein are required to effect the process (4–6). For this reason, the researcher can focus more on the protein-lipid interaction and the biophysical aspects of the lipid bilayer.

In viral membrane fusion systems, special glycoproteins located on the viral envelope are required to mediate membrane fusion (7,8). The major region of viral spike glycoproteins that interacts with lipid bilayers of the host is called the fusion peptide (FP). Another membrane-associated part of viral spike glycoproteins, the transmembrane domain (TMD), is permanently in the viral lipid bilayer. FPs interact with the host lipid bilayer only upon activation of the fusion process. Many FPs, such as those of influenza and HIV, are located at the N-terminus of the fusion subunit of the viral spike glycoproteins, whereas others, such as those of Ebola and avian sarcoma leukosis viruses, are internal sequences of the respective fusion proteins (9). Despite their different locations and different triggering mechanisms, FPs are critical for mediation of membrane fusion.

It has been shown that insertion of FPs into the host membrane is critical for membrane fusion in that it can perturb the structure of the membrane. In previous studies, using electron-spin resonance (ESR), we measured the ordering in the headgroup and acyl chain regions in the lipid bilayer after influenza hemagglutinin (HA) FP insertion (10). Our studies showed that the insertion of HA FP in dimyristoylphosphatidylcholine or 1-palmitoyl-2-oleoyl-*sn*-glycero-3-phosphocholine (POPC) bilayers results in an increase of lipid order at pH 5 but not at pH 7. This result was consistent with experiments on planar bilayers using Fourier transform infrared spectroscopy (FTIR) (11,12). The advantage of the ESR experiments is that they allow determination of the depth of the FP effect in the lipid bilayer.

Compared to HA FP, the structure of HIV gp41 FP is more plastic. The HIV FP consists of 15 apolar residues, followed by another eight moderately polar residues. The FP can adopt either an α-helical structure or a β-sheeted structure, depending on the composition of the lipid, the peptide/lipid (P/L) ratio, and the temperature, etc. How lipid composition affects the secondary structure, and whether the helical structure or the aggregation structure mediates membrane fusion, are under debate. A recent article suggests that cholesterol is the critical factor: the FP adopts an α-helical structure when the cholesterol concentration is $<30\%$ and a β-sheet structure when the cholesterol concentration is $>30\%$. It also showed that both structures induce membrane fusion, though the β-sheet structure does so more efficiently, especially with regard to content mixing, i.e., the fusion of the inner leaflets of two membranes (13).

How the HIV FP perturbs the membrane structure remains unknown, and in this study, we show that the HIV FP increases the order of the lipid bilayer in both α-helical

Submitted July 24, 2013, and accepted for publication November 13, 2013.

*Correspondence: jhf3@cornell.edu

Editor: Mei Hong.

0006-3495/14/01/0172/10 $2.00

http://dx.doi.org/10.1016/j.bpj.2013.11.027

and β-sheet structure. However, the effect of the β-sheet conformer extends more deeply into the hydrophobic region of the bilayer. Our results, when compared with those on HA FP (10), suggest that the ordering effect of FPs is common across different viruses and is a requirement for gp41-FP-mediated membrane fusion.

MATERIALS AND METHODS

Materials

The lipids POPC and 1-palmitoyl-2-oleoyl-*sn*-gycero-3-phosphoglycerol (POPG), the chain spin labels 5PC and 14PC, and a headgroup spin label, dipalmitoylphospatidyl-tempo-choline (DPPTC), were purchased from Avanti (Alabaster, AL). Cholesterol was purchased from Sigma (St. Louis, MO). The peptide that corresponds to the first 23 residues of the N-terminal sequence of the LAV_{mal} strain HIV-1 gp41 and its V2E mutant were synthesized by SynBioSci (Livermore, CA). Its I4C, A15C, and A21C mutants were synthesized by Peptide 2.0 (Chantilly, VA). The structure of the spin-labeled lipids and the sequences of the peptides are shown in Fig. 1.

Sample preparation

The desired amount of POPC, POPG, cholesterol, and 0.5% (mol/mol) spin-labeled lipids in chloroform were mixed well and dried by N_2 flow. The mixture was evacuated in a vacuum drier overnight to remove any trace of chloroform. To prepare multilamellar vesicles (MLVs), the lipids were resuspended and fully hydrated using 1 mL of pH 7 buffer (50 mM Tris, 150 mM NaCl and 0.1 mM EDTA) at room temperature (RT) for 2 h. The desired amount of stock solution of the FP (1 mg/mL in DMSO) was added into the lipid dispersion. After 20 min incubation, the dispersion was spun at 13,000 rpm for 10 min to collect the pellet. The pellet was transferred to a quartz capillary tube for ESR measurement.

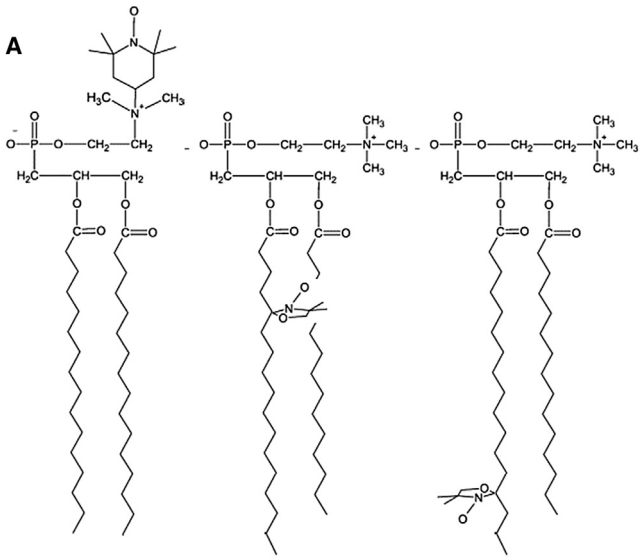

FIGURE 1 (*A*) Structures of spin-labeled lipids DPPTC, 5PC, and 14PC. (*B*) Peptides used in this study, with mutations shown in bold letters.

Peptide spin labeling

The desired amounts of FPs with cysteine mutations, I4C, A15C, and A21C, with a -GGGKKKK sequence in their C-termini were dissolved in 50:50 acetonitrile:buffer and mixed with 10-fold excess (S-(2,2,5,5-tetramethyl-2,5-dihydro-1H-pyrrol-3-yl)methyl methanesulfonothioate) dissolved in the same solution overnight in the dark at RT, as described previously (12,13). The spin-labeled peptides were purified using high-performance liquid chromatography. The spin-labeled peptides were confirmed by ESR and mass spectrometry. The spin-labeled peptides, which are designated as I4R, A15R, and A21R, were lyophilized and kept at $-80^{\circ}C$ before the experiments.

ESR spectroscopy and nonlinear least-squares fit of ESR spectra

ESR spectra were collected on an E500 ESR spectrometer (Bruker Instruments, Billerica, MA) at X-band (9.5 GHz) using an N2 Temperature Controller (Bruker Instruments). For low-temperature ESR, each sample (~1 mg lipids with labeled peptides at 0.01 P/L ratio) was rapidly frozen in thin capillaries by quick submerging in liquid nitrogen before measurement.

The ESR spectra from the labeled lipids were analyzed with the NLLS fitting program based on the stochastic Liouville equation (14,15) using the microscopic-order-macroscopic-disorder model as in previous studies (10,16–19). Two sets of parameters that characterize the rotational diffusion of the nitroxide radical moiety in spin labels are generated. The first set consists of $R_{\perp}$ and $R_{||}$, which are the rates of rotation of the nitroxide moiety around a molecular axis perpendicular and parallel, respectively, to the preferential orienting axis of the acyl chain. The second set consists of the ordering tensor parameters, S_0 and S_2, which are defined as follows: $S_0 = <D_{2,00}> = <1/2(3\cos^2\theta - 1)>$, and $S_2 = <D_{2,02} + D_{2,0-2}> = <\sqrt{(3/2)}\sin^2\theta\cos 2\varphi>$, where $D_{2,00}$, $D_{2,02}$, and $D_{2,0-2}$ are the Wigner rotation matrix elements and θ and φ are the polar and azimuthal angles for the orientation of the rotating axes of the nitroxide bonded to the lipid relative to the director of the bilayer, i.e., the preferential orientation of lipid molecules (10,15), and the angular brackets imply ensemble averaging.

S_0 indicates how strongly the chain segment to which the nitroxide is attached is aligned along the normal to the lipid bilayer, which is strongly correlated with hydration/dehydration of the lipid bilayers (16). S_2 is the measurement of the molecular nonaxiality of the motion of the spin label. It was found to be much smaller than S_0, with much less sensitivity to changes in the bilayer structure in our studies. Therefore, S_0 is the more important parameter for this study. The estimated error of S_0 from the NLLS fit for the spectra (the typical standard deviation obtained in the fitting) is $\sim \pm 0.01$.

We also performed pulsed ESR experiments on the labeled peptides on frozen samples at 60 K (20), and these are discussed in the Supporting Material.

RESULTS

The binding of gp41 FP increases the ordering of membranes

To examine the perturbation of the lipid bilayers by gp41 FP, we incorporated three different spin-labeled lipids into the

membranes. DPPTC has a tempo-choline headgroup and the spin is sensitive to changes of environment at the headgroup region. 5PC and 14PC have a doxyl group in the C5 and C14 positions, respectively, of the acyl chain. They are sensitive to the change of environment in the hydrophobic acyl chain region at different depths. These three spin-labeled lipids have been used before, and their efficacy in detecting changes in membrane structure has been validated (10,16–19).

We first studied the effect of HIV FP on POPC/POPG 4:1 MLVs. We used this lipid composition because its structure and fusogenicity have been well defined (13). In that study, the secondary structure of the FP was examined by circular dichroism (CD), and the fusion activities were examined by Förster resonance energy transfer (FRET). The FP adopts an α-helical structure in membranes containing 0% cholesterol and has a moderate membrane fusion activity. As a control, we used a V2E FP mutant, which has been shown to be nonfusogenic (21). As shown in Fig. 2, *A–C*, when the P/L ratio increases from 0 to 10×10^{-3}, the S_0 of the DPPTC and 5PC spin labels at 37°C and pH 7 increases significantly, whereas V2E exhibited almost no increase of S_0 in the headgroup region and no change in the acyl region at all. However, no change of S_0 in the core hydrophobic region (14PC) was observed even for wild-type HIV FP. The rotational diffusion rates, $R_\perp$ and $R_{||}$, and S_0 of 5PC, 14PC, and DPPTC in these conditions are listed in Tables S1–S6 in the Supporting Material.

This result is consistent with the study on influenza HA FP using the same method but on a different lipid mixture (10). When in its activated condition at pH 5, HA FP induces an increase of S_0 of the headgroup and the shallower hydrophobic region, whereas it has no effect on the deeper hydrophobic region. It is not surprising that these two peptides exhibit a similar effect on the lipid structure, because they share a series of features and serve similar functions (7,22).

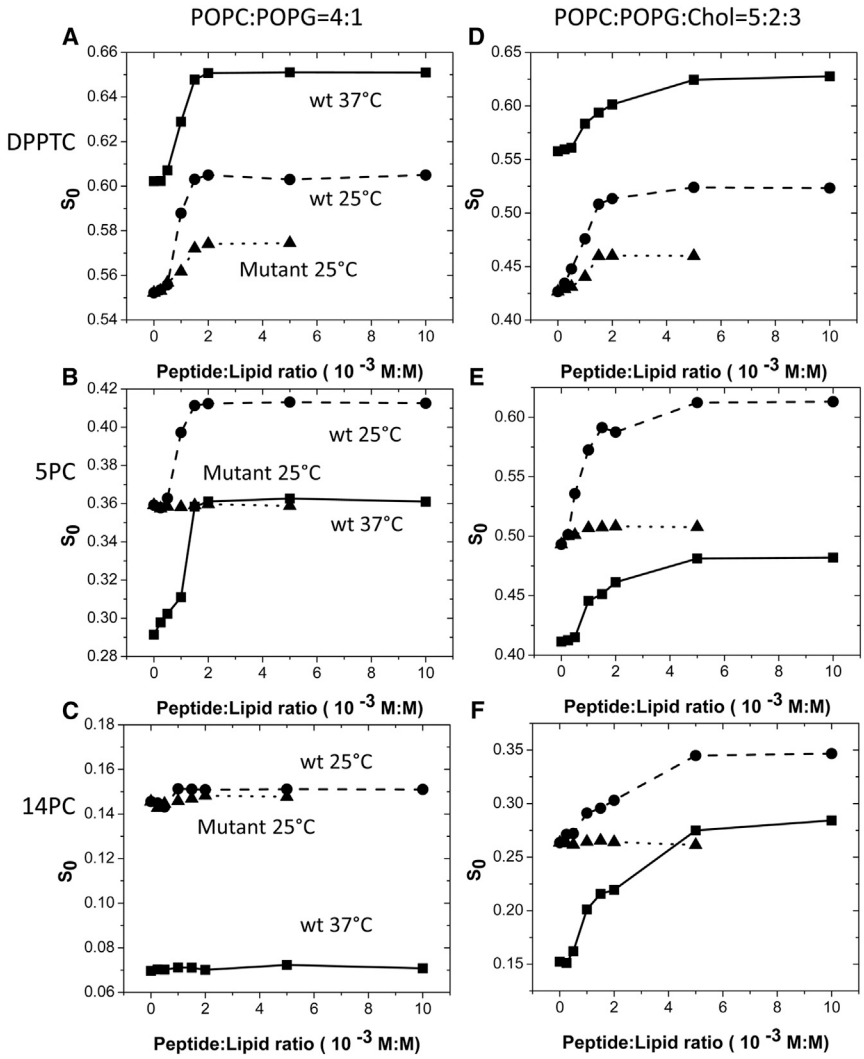

FIGURE 2 Plot of order parameters of DPPTC (*A* and *D*), 5PC (*B* and *E*), and 14PC (*C* and *F*) in POPC/POPG 4:1 (*A–C*) and POPC/POPG/Chol 5:2:3 (*D–F*) mixtures versus the P/L ratio of wild-type HIV FP at 25°C (*circles and dashed lines*) and 37°C (*squares and solid lines*) and mutant V2E at 25°C (*triangles and dotted lines*).

β-Sheeted conformers perturb the membrane structure deeper in the hydrophobic region

A previous study (13) shows that the FP adopts a β-aggregated conformation in lipid bilayers of POPC/POPG/Chol 5:2:3, and that the lipid mixing ratio (i.e., the extent of mixing of membrane lipids) induced by the β-sheeted conformer is higher than that induced by the α-helical conformer (~70% vs. 50%). We studied the effect of the β-sheeted conformers of the gp41 FP on the bilayers. As shown in Fig. 2, *D–F*, when the P/L ratio increases from 0 to 10×10^{-3}, the S_0 of DPPTC, 5PC, and 14PC increases from 0.558 to 0.628, 0.411 to 0.482, and 0.152 to 0.284, respectively. The rotational diffusion rates, $R_\perp$ and $R_{||}$, and S_0 of 5PC, 14PC, and DPPTC in these conditions are listed in Tables S7–S12.

One clear difference between the effects of α-helical and β-sheeted conformers is that the β-sheeted conformer affects the lipid structure deeper in the hydrophobic region. This effect is exhibited at both 25°C and 37°C. Neither the HIV FP α-helical conformer nor the influenza HA FP, which also adopts a mostly helical structure, exhibits any effect in the core hydrophobic region.

Even in the headgroup region and the nearer hydrophobic region, the β-sheeted conformer exhibits a larger perturbation to the lipid than does the α-helical conformer. At 37°C, the $\Delta S_{0,max}$ for DPPTC in the membrane containing 0 mol % cholesterol is 0.051, whereas in the membrane containing 30 mol % cholesterol it is 0.070. The corresponding $\Delta S_{0,max}$ values for 5PC are 0.069 and 0.071, respectively. The difference at the lower temperature is even larger. At 25°C, the $\Delta S_{0,max}$ for DPPTC in the membrane containing 0 mol % cholesterol is 0.053, whereas in the membrane containing 30 mol % cholesterol it is 0.097. The corresponding $\Delta S_{0,max}$ values for 5PC are 0.053 and 0.12, respectively (Table 1).

The pattern of the extent of perturbation versus P/L ratio is also different. For the helical conformer, the increase in order parameter was fitted well with a typical sigmoidal function using Origin (OriginLab, Northampton, MA), whereas for the β-sheeted conformer, the perturbation versus P/L ratio curve is more complex. It appears to exhibit a two-stage increase. This may be explained by the structural and aggregative transition for the β-sheeted conformers. This two stage perturbation is clearest in the spectra of 14PC.

The other difference is that the β-sheeted conformers affect the membrane structure at a lower P/L ratio, indicating that the β-sheeted conformation is more efficient for inducing the change in the membrane structure. However, the $C_{1/2}$, defined as the P/L ratio that induces 50% of the $\Delta S_{0,max}$, is higher than that of the α-helical conformer (Table 1). This also suggests a more complex dynamic of the β-sheet conformer.

TABLE 1 Comparison of structures, fusion activities, and membrane perturbations by HIV gp41 FP in POPC/POPG membranes with different cholesterol concentrations

	Mainly α-helix			Mainly β-sheet
	0% Cholesterol	10% Cholesterol	20% Cholesterol	30% Cholesterol
α-helical (%)[a]	79	78	62	9
β-sheet %[a]	1	1	6	47
Lipid mixing ratio (%)[a]	55	60	60	70
Lipid mixing rate (10^{-3}%/s)[a]	3.8	9.9	8.7	22.6
Contents mixing/ leakage ratio (%)[a]	22	*33*	70	NA
ΔS_0 for DPPTC (G)	0.0488	0.0482	0.0629	0.0967
$C_{1/2}$ for DPPTC (10^{-3} M/M)	0.875	0.821	0.887	0.94
ΔS_0 for 5PC (G)	0.0533	0.0618	0.0673	0.120
$C_{1/2}$ for 5PC (10^{-3} M/M)	0.835	0.861	0.922	0.704
ΔS_0 for 14PC (G)	0.0054	0.0065	0.0062	0.0832
$C_{1/2}$ for 14PC (10^{-3} M/M)	NA	NA	NA	0.862 2.61

The α-helical and β-sheeted percentages are calculated from the CD experiments at 10×10^{-3} P/L ratio. The lipid mixing ratio and contents mixing/leakage ratio are defined as the ratio of maximal fluorescence intensity increase induced by HIV FP to maximal fluorescence intensity increase induced by detergent. The lipid mixing rate is defined as the initial lipid mixing ratio percentage per second. ΔS_0 is the difference of order parameter of membranes with and without FP binding at 10×10^{-3} P/L ratio. $C_{1/2}$ is defined as the P/L ratio that induces 50% of ΔS_0.
[a]Data calculated from results of Lai et al. (13).

Spectra from labeled peptides

To further investigate the structural transition as the P/L ratio in the membrane increases, we spin-labeled the A15C mutation of the FP and measured the ESR spectra in membranes containing both 0 mol % cholesterol and 30 mol % cholesterol. The peptide was prepared containing a highly polar and flexible sequence, -GGGKKKK (cf. Fig. 1), at the C-terminus to increase the solubility of the peptide; this is widely used and it has been shown not to affect the P/L interaction (13,23,24).

As shown in Fig. 3, the ESR spectra of A15R at RT in membranes containing 0 mol % cholesterol are nearly identical to each other over the P/L ratio range of 0.5×10^{-3} to 10×10^{-3}, indicating that the FP remains in a very similar conformation. This is consistent with the α-helical monomer conformation expected over this range. However, when the spectra for FP in membranes containing 30 mol % cholesterol are compared, one finds that those for 1.5×10^{-3} to 10×10^{-3} P/L ratio are similar, but that they are significantly different from that for 0.5×10^{-3} P/L ratio. In fact, the latter is almost identical to the comparable spectrum at 0 mol % cholesterol. Previous studies have shown that for 33 mol % cholesterol, the FP can adopt the β-sheet structure involving FP aggregation when the P/L ratio is $>1.25 \times 10^{-3}$ (25). Thus, we attribute the substantial broadened component seen for P/L ratios greater than this to the β-sheet conformers, with the nitroxides of the aggregated peptides yielding significant broadening from their

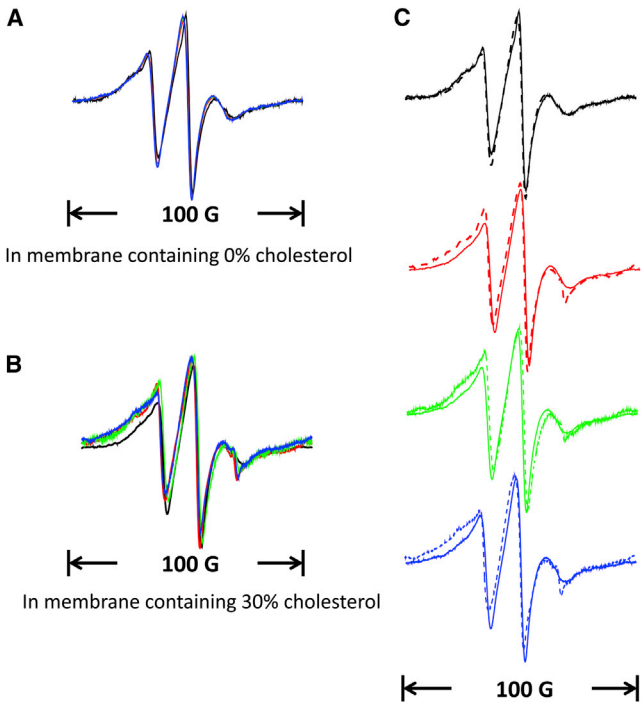

FIGURE 3 ESR spectra of A15R HIV FP in POPC/POPG 4:1 (*A*) and POPC/POPG/Chol 5:2:3 (*B*) MLVs. (*C*) Superposition of spectra in *A* and *B*, grouped by P/L ratio for POPC/POPG 4:1 (so*lid lines*) and POPC/POPG/Chol 5:2:3 (*dashed lines*) with FPs at P/L ratios of 0.5×10^{-3} (*black*), 1.5×10^{-3} (*red*), 5×10^{-3} (*green*), and 10×10^{-3} (*blue*), at 25°C.

dipolar interactions. Pulsed ESR experiments of frozen samples shown in Fig. S1 yield a dramatic decrease in phase memory time, T_m, versus cholesterol composition, consistent with such aggregation providing a strong relaxation mechanism due to the dipolar interactions.

The sharp signal seen in these spectra is possibly a small amount of FP in the aqueous phase. This is not seen in any of the 0%-cholesterol spectra. Since one expects the 0%-cholesterol membranes to be in the liquid-disordered phase and the 30%-cholesterol membranes to be in the liquid-ordered phase and therefore less accepting of the peptide, this spectral feature seems to be a reasonable consequence of reduced solubility of the FP. We do note that there is an underlying broad component in the spectra with 0% cholesterol, but its source is uncertain. Also, our results with 30% cholesterol indicate that a certain amount of α-helical monomer persists in these membranes. Note that CD experiments show that there is an ~10% content of α-helical conformer in 30%-cholesterol membranes at 10×10^{-3} P/L ratio (cf. Table 1). This structural transition of the FP from low to high P/L ratio in 30%-cholesterol membranes could lead to an explanation as to why the FP perturbs the membranes containing 30 mol% cholesterol in two stages, as discussed in the previous paragraph.

Overall, our observations indicate that the conformational behavior of the spin-labeled FP is quite similar to that of the unlabeled FP, because both ESR and CD (13) show aggregation for 30%-cholesterol samples.

The nonfusion mutant is unable to perturb the hydrophobic region

To determine whether the perturbation of the membrane by the FP is significant for the function of the FP, we used a V2E mutant as a control. The V2E mutant is known to lack fusogenicity (26). The peptide was incorporated into membranes containing both 0 mol % and 30 mol % cholesterol. As shown in Fig. 2, whereas the V2E mutant has a much smaller effect in the headgroup region, it has essentially no effect on the lipid structure in the acyl chain region. This result confirms that the perturbation of the membrane by the FP is related to its fusogenicity. The rotational diffusion rates, $R_\perp$ and $R_{||}$, and S_0 of 5PC, 14PC, and DPPTC in these conditions are listed in Tables S16–S21.

β-Sheeted conformers have a stronger effect on the structure of the membrane

To further compare the membrane ordering effect in membranes with different cholesterol concentrations, we repeated our experiments in membranes containing 10 mol % and 20 mol % cholesterol. As shown in Fig. S2, the FP increases the lipid order in the headgroup and the upper hydrophobic region, but not in the lower hydrophobic region. The change of S_0 for DPPTC and 5PC is similar to that in the membrane containing 0 mol % cholesterol and smaller than that in the membrane containing 30 mol % cholesterol. No perturbation to the core hydrophobic region was observed. These results are consistent with the hypothesis that the α-helical conformers have practically no effect on the lipid order in the lower hydrophobic region.

The HIV FP also affects the structure of natural lipid membranes

To determine how the HIV FP perturbs a natural lipid membrane, we examined its effect in MLVs made from bovine liver lipid extract (LLE). The LLE contains not only PG but also significant amounts of other negatively charged lipids, such as phosphoinositol (PI) and phosphoserine (PS). The concentrations of PI + PE and PS are ~32% and 6% (Avanti http://www.avantilipids.com (19)), close to those in T-cell membranes infected by HIV (27). Thus, it is a suitable representative natural lipid. The LLE contains ~7% cholesterol (Avanti, http:// www.avantilipids.com). As shown in Fig. S3, the FP increases the lipid order from ~0.18 to 0.22 in the headgroup region and from ~0.44 to ~0.49 in the upper hydrophobic region, but it has no effect on the lower region. The perturbation is thus similar to that for the 0%-cholesterol membrane, which is consistent with the hypothesis that the helical conformers affect only the

upper hydrophobic region. The rotational diffusion rates, $R_\perp$ and $R_{||}$, and S_0 of 5PC, 14PC, and DPPTC in these conditions are listed in Tables S13–S15.

Temperature change modulates the change in membrane perturbation

To determine whether temperature affects the FP's ability to perturb membrane structure, we measured the ESR spectra of lipid spin labels in membranes containing 0 mol % cholesterol and 30 mol % cholesterol with and without HIV FP at 10×10^{-3} P/L ratio at different temperatures between 20°C and 37°C. The order parameter difference, ΔS_0, was calculated as the S_0 of the membrane with HIV FP at 10×10^{-3} P/L ratio minus the S_0 of the membrane without HIV FP. As shown in Fig. 4, the ability of the FP to perturb the membrane decreases with the decrease in temperature, which is consistent with the fact that fusogenicity decreases when the temperature decreases (28).

The exception is for 5PC in the membrane containing 30 mol % cholesterol, where the ΔS_0 initially increases with the decrease in temperature from 37°C to 25°C, then decreases when the temperature goes below 25°C. This would appear to be abnormal, but it can be explained. The β-sheeted conformers drive the membrane fusion partly by perturbing the lower hydrophobic region. As the temperature decreases, its ability to perturb the lower hydrophobic region could decrease because of its reduced ability to penetrate into the deeper region due to the increased density. Instead, it stays more in the upper hydrophobic region and gains increased ability to perturb this region. Since perturbing the deeper membrane region is more effective in driving membrane fusion than perturbing the shallower region, the overall fusogenicity still decreases when the temperature decreases.

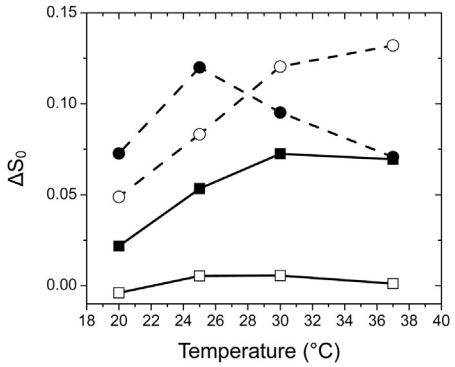

FIGURE 4 Difference of order parameters (ΔS_0) versus temperature for 5PC in POPC/POPG 4:1 (*solid squares*), 14PC in POPC/POPG 4:1 (*open squares*), 5PC in POPC/POPG/Chol 5:2:3 (*solid circles*), and 14PC in POPC/POPG/Chol 5:2:3 (*open circles*). Solid lines and dashed lines are used to represent POPC/POPG 4:1 and POPC/POPG/Chol 5:2:3 membranes, respectively, for better display purposes.

β-Sheeted conformers insert more deeply than helical conformers

The membrane insertion of the α-helical conformers was determined by power-saturation ESR for I4C, L7C, I12C, and A15C spin-labeled HIV FPs (13). The results indicate that the helical conformers insert into the membrane shallowly and almost horizontally on the interface of the hydrophilic headgroup region and the hydrophobic region.

We exploited low-temperature ESR to determine the relative insertion depth of the β-sheeted conformers in the membrane. When the temperature decreases to 90 K, the spectra of frozen samples of labeled FP reach the rigid limit. The $2A_{zz}$ is directly measurable at the magnetic frequency between the minimum of the high field and the maximum of the low field. With the exception of polarity, all factors that affect the value of outer splitting, $2A_{zz}$, are frozen in the rigid limit (20). A larger $2A_{zz}$ indicates a more hydrophilic environment and a smaller $2A_{zz}$ indicates a more hydrophobic environment. The hydrophobic environment indicates a deeper region in the bilayer. Thus, we correlated the $2A_{zz}$ value with the insertion depth.

We spin-labeled three different positions of the FP, I4C, A15C, and A21C (cf. Fig. 1), which are located at the N-terminal, middle, and C-terminal regions of the α-helix, respectively, based on the NMR structure in sodium dodecyl sulfate micelles (29). We mainly compare the spectra of those peptides at 5×10^{-3} P/L ratio in membranes containing 20 mol % and 30 mol % cholesterol. We preferred the membrane containing 20 mol % cholesterol over that for 0 mol % cholesterol, because we wanted to minimize the difference of hydrophobicity caused by different concentrations of cholesterol. Since the FP still adopts an α-helical structure in membranes containing 20 mol % cholesterol, we can still compare the insertion depth of these two conformers. We rapidly froze the samples to avoid structural change during freezing. Solid-state NMR experiments indicate that the low temperature does not change the structure of HIV FP (30).

As shown in Fig. S4, the $2A_{zz}$ value for A15R in solution is 73.9 G, but when A15R binds to a membrane containing 0 mol % cholesterol, the $2A_{zz}$ value decreases to 72.0 G. The $2A_{zz}$ values in membranes containing 10 mol % and 20 mol % cholesterol are similar to that for 0 mol % cholesterol (71.8 G and 71.7 G, respectively). However, the $2A_{zz}$ value decreases significantly, to 69.3 G, when the peptides bind to a membrane containing 30 mol % cholesterol, suggesting a significantly more hydrophobic environment for the spin. We attribute this change to deeper insertion.

In Table 2, we compare the $2A_{zz}$ values of I4R, A15R, and A21R in solution for membranes containing 20 mol % and 30 mol % cholesterol. All membrane-bound peptide mutants show smaller $2A_{zz}$ values than the corresponding unbound mutants. We found that the $2A_{zz}$ values for peptides in 30%-cholesterol membranes are all smaller than the values

TABLE 2 $2A_{zz}$ values for three spin-labeled peptides in buffer and in membranes containing 20 mol % or 30 mol % cholesterol at the rigid limit

Mutants	$2A_{zz}$ in pH 7 buffer (G)	$2A_{zz}$ in POPC/POPG/Chol 60:20:20 (G)	$2A_{zz}$ in POPC/POPG/Chol 50:20:30 (G)
I4R	73.7	72.5	71.6
A15R	73.7	72.1	69.2
A21R	73.9	71.7	69.3

Values of $2A_{zz}$ for I4R, A15R, and A21R were calculated from X-band CW-ESR spectra recorded at 90 K.

for those in 20%-cholesterol membranes, which indicates deeper insertions for all three spin-labeled positions. However, the difference for I4R is significantly smaller than those for A15R and A21R. This may indicate that I4 is located in a shallower position than are A15 and A21. The β-sheeted conformer may insert into the membrane with a tilt angle, with its C-terminus inserting deeper than its N-terminus, which is consistent with an FTIR study on the insertion angle of β-sheeted HIV FP (31).

DISCUSSION

The order parameter S_0 represents the axial ordering of lipid molecules in bilayers, which originates from the lateral restoring torques exerted on each lipid molecule by its neighboring lipid molecules. The restoring torque is associated with an orienting potential in the bilayer and is minimized when the angle between the primary axis for a chain segment (or a headgroup) and the normal to the bilayer is equal to zero. The restoring torque is related to, but different from, the lateral pressure that is frequently cited (32,33). The restoring torque induces reorientation of the lipid molecules, whereas the lateral pressure induces their compression. Molecular interactions between lipid molecules are dominated by van der Waals forces in the acyl-chain region and by ionic forces generated by hydrogen bonding in the headgroup region.

We found that the fusogenicity of the HIV FP is strongly correlated with the membrane ordering induced by the FP. The nonfusogenic V2E mutant has a much smaller effect on the order of the headgroup region, and it has basically no effect on the ordering of the hydrophobic region. Its lack of fusogenicity strongly suggests the importance of membrane ordering for membrane fusion. Previous studies have shown that influenza FPs increase membrane order, and that the ordering effect is required for their fusogenicities (10,11). Therefore, the membrane ordering effect appears to be a general phenomenon for the FP-mediated membrane fusion in viral entry.

The plasticity of HIV FP is a key feature that differentiates the HIV and influenza FPs. Although influenza HA FP takes on different structures at different pH values and environments, either a boomerang shape (34) or a tight hairpin (35), it adopts a mainly helical structure. This difference is significant, but not as large as that seen for HIV gp41 FP. Although the membrane fusion associated with HIV viral entry is triggered by ligands, i.e., the receptors and coreceptors on the target membrane, instead of by acidity, the structure of HIV FP is not affected by pH in the physiological range. However, the structure of HIV FP is strongly affected by the lipid composition, especially the concentration of cholesterol. Its structure changes dramatically, from α-helix at low cholesterol concentration to β-sheet at high cholesterol concentration (i.e., >30%). Thus, the mechanism of HIV FP-mediated membrane fusion is more complex than that of the influenza FP-mediated membrane fusion.

The HIV FP-induced ordering effect on the membrane is strongly correlated with the secondary structure of HIV FP. In Fig. 5, we show several key factors together to better compare the structure, fusogenicity, and membrane perturbation at different cholesterol concentrations. More parameters are listed in Table 1. The β-sheet percentage of the FP and the lipid mixing rate with the unit %/s were calculated from CD and FRET experiments in a previous study (13), in which fusogenicity was examined by a lipid mixing experiment. The addition of FP induces lipid mixing between these two vesicles, and the fusion between the membranes can be monitored by increased fluorescence intensity due to the increase in distance between the FRET donor and receptor pairs because of membrane fusion. Two parameters can be drawn from such an experiment. The lipid mixing ratio is the ratio of the final fluorescence intensity increase after peptide induction to the fluorescence intensity increase when detergent is added into the system and totally disrupts the membrane. Thus, it reflects the extent of FP-mediated membrane fusion. The lipid mixing rate is the initial rate of the lipid mixing induced by the FP, defined as the intensity increase per second. Thus, it reflects the dynamics of the membrane fusion.

Although the difference of the lipid mixing ratio (in Table 1) for membranes containing different cholesterol

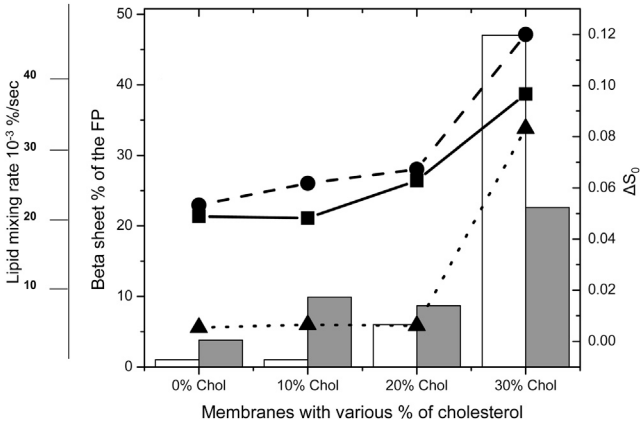

FIGURE 5 Comparison of the β-sheet % (*white columns*), lipid mixing rate (*gray columns*), and ΔS_0 for DPPTC (*squares*), 5PC (*circles*), and 14PC (*triangles*) with FP binding at 10×10^{-3} P/L ratio at 37°C in membranes containing 0%, 10%, 20%, and 30% cholesterol.

concentrations is substantial, the difference for the lipid mixing rate is more significant. That is, there is not much difference between the lipid mixing rate for membranes containing 0 mol %, 10 mol %, and 20 mol % cholesterol, but the rate for a 30 mol % cholesterol membrane is much higher. The membrane fusion fusogenicity is well correlated with structural differences. This indicates that even though both helical and β-sheeted structures induce membrane fusion, the β-sheeted conformer functions in a faster and more efficient way than the α-helical conformer.

We found in this ESR study that the HIV FP perturbs the membrane order in two ways, which correspond to its two different conformations. The α-helical conformers affect the membrane order in the headgroup and upper hydrophobic regions, whereas the β-sheeted conformers affect the membrane order in the headgroup and both the upper and lower hydrophobic regions. The mode of perturbing the membrane for the α-helical conformer is similar to that of the influenza FP. This may not be surprising, since they both adopt α-helical structure and insert modestly into the membrane (13,23,29,34).

The β-sheeted conformer increases the ordering of the headgroup and the upper hydrophobic region to a greater extent than does the α-helical conformer, and its ordering effect reaches more deeply into the hydrophobic region. The facts that both α-helical and β-sheeted conformers promote membrane fusion and both perturb membrane structure in the hydrophobic region suggest that the ordering effect is a prerequisite for membrane fusion. However, their fusogenicities are well correlated with the extent and depth of the ordering effect. The finding that the β-sheeted conformer inserts more deeply into the membrane is consistent with low-temperature solid-state NMR studies on β-sheeted HIV FP (36) and electron ESR studies on α-helical HIV FP at RT (13).

Our results are consistent with previous studies on influenza HA FP and the TMD of HA by ESR (10,19) and FTIR (11,24) and on HIV FP by fluorescence anisotropy (37). However, they would appear to be different from the x-ray diffraction study (38) (see also the FTIR work (31)), which indicates a disordering effect on the lipid acyl chain. First, we note that the ESR experiments have all been performed on vesicle dispersions, whereas the x-ray study was on oriented multilayers. Since vesicle dispersions are randomly oriented throughout the sample, the ESR experiment senses a uniform distribution of local directors but enables us to measure the magnitude of the local ordering, S_0. This is the essence of the microscopic-order-macroscopic-disorder model (14). Thus, the effect of FP insertion could disrupt the macroscopic alignment of oriented multilayers, but such directional disruption is not detectable in the ESR experiment on multilayers; only the order parameter, S_0 (and S_2), is detectable, which may still increase despite local mosaicity introduced in terms of the direction of ordering. Second, the difference might also be generated by differences in composition of the lipid and the P/L ratio in the experiments, as well as the timescale of the methods. For example, in x-ray diffraction, the peptides are trimerized and the P/L ratios are 48×10^{-3} and 144×10^{-3} for FP monomers, which is much greater than in our experiments. The lipid in the x-ray experiment generally lacked negatively charged lipid, except for the very complicated LM3 mixture (i.e., POPC/POPE/POPS/PI/SM/Chol 10:5:2:1:2:10), in which the FP does not have well-defined secondary structure.

The increase of S_0 is attributed to a dehydration effect (16). Dehydration of bilayers is the process of loosely bound water moving from the interbilayer region to the bulk water phase. It has been suggested that the hydrophobic interaction between exposed acyl chains in the region of closely apposed membranes is responsible for the attractive forces between the fusing membranes, and that the exposure of the hydrophobic interior of the bilayers is caused by stresses in the bilayers (39,40). Thus, dehydration is the required step to remove the energy barrier between two membranes and allow them to come into proximity.

When the FP binds to the outer leaflet of the host membrane, the outer layer becomes more condensed and more solidlike, which tends to shrink its area. Since the two monolayers are mechanically coupled, as they cannot slide relative to each other, condensing the outer layer will generate a compressive force on the inner layer and thus promote a negative curvature of the membrane. Both theoretical schemes to explain membrane fusion and experimental results suggest that the membrane fusion efficiency is affected by membrane curvature, which may be related to stalk intermediate formation (41–44). Thus, a greater dehydration effect generates greater negative curvature and increases the efficiency of membrane fusion, which explains why β-sheeted conformers possess high fusogenicity (Fig. 6). In Fig. 6, we draw the FP in β-sheet conformation

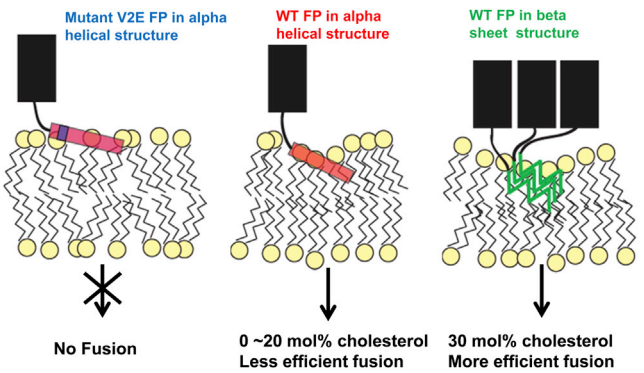

FIGURE 6 Schematic representation of the modes of HIV gp41 FP insertion into lipid bilayers, and its effects on membrane order and fusion activities. The FP in β-sheet conformation is represented as a trimer simply because gp41 is a trimer. Its real stoichiometry during the membrane fusion process has not been confirmed. FP conformations shown are α-helical (*red*), β-sheet (*green*); the gp41 ectodomain is *black*.

as a trimer simply because gp41 is trimeric. Its real stoichiometry during the membrane fusion process has not been confirmed.

HIV viral entry has been shown to require high cholesterol concentration, as the depletion of cholesterol greatly reduces the infection rate (45). It has also been shown that the target membrane for HIV viral entry is the endosomal membrane, which has higher cholesterol concentration than plasma membranes (46). In the cell membrane, the cholesterol does not distribute uniformly, and it often concentrates around a raft region (47). HIV FP has a tendency to associate with rafts, but this should not be directly relevant for our study using model membranes. It is possible that in the physiological scenario, most of the FPs associate with the raft and form the β-sheeted conformation and fewer FPs are in the nonraft lipid domain and remain in the α-helical conformation. This distribution would increase the overall lipid mixing rate.

The possible transition between α-helical structure and β-sheet structure is suggested to occur in the fusion process (13,41). In the scenario of membrane fusion mediated by full-length gp41, the transition is more plausible. Interaction between the TMD and FP of influenza HA (48,49) and HIV gp41 (50) has been reported. In our study, we found that spin labels in membranes with simultaneous binding of TMD and FP of HIV gp41 exhibit a different line shape compared to those from membranes with TMD or FP alone (unpublished data), which strongly suggests the importance of TMD-FP interaction in membrane fusion. It is rational to postulate that the FP interacts with the TMD in an α-helical structure. The TMD of influenza HA also induces a highly ordered domain in the membrane. Therefore, a transition from the β-sheet conformation to the α-helix conformation will be facilitated by the TMD. The initialization of lipid mixing and finalizing the pore opening could be mainly achieved by the two different conformations: the β-sheet conformation is better for lipid mixing, and the α-helix conformation is better for pore opening through interacting with the TMD.

CONCLUSIONS

We found that the binding of HIV gp41 FP to POPC/POPG bilayers containing various cholesterol concentrations increases the order of the headgroup and the acyl chain regions. The β-sheeted conformer, which is dominant in membranes containing $\geq$30 mol % cholesterol, has a greater and deeper membrane ordering effect than the α-helical conformer, which is dominant in membranes containing $<$30 mol % cholesterol. This is correlated with their fusogenicities. The increase of lipid ordering suggests a dehydration effect that is required for the initiation of viral membrane fusion. This increase in ordering upon binding of HIV FP is similar to that previously observed for influenza HA FP, suggesting that membrane ordering is a common prerequisite for viral membrane fusion.

SUPPORTING MATERIAL

Four figures, 22 tables and Reference (51) are available at http://www.biophysj.org/biophysj/supplemental/S0006-3495(13)01262-9.

We thank Dr. Boris Dzikovski and Dr. Zhichung Liang for help in data analysis and discussion of this research.

This work was supported by National Institutes of Health grants NIH/NIBIB R01EB003150 and NIH/NIGMS P41GM103521.

REFERENCES

1. Lang, T., and R. Jahn. 2008. Core proteins of the secretory machinery. *In* Pharmacology of Neurotransmitter Release. T. Südhof and K. Starke, editors. Springer-Verlag, Berlin, pp. 107–127.
2. Sudhof, T. C., and J. E. Rothman. 2009. Membrane fusion: grappling with SNARE and SM proteins. *Science.* 323:474–477.
3. Rizo, J., and C. Rosenmund. 2008. Synaptic vesicle fusion. *Nat. Struct. Mol. Biol.* 15:665–674.
4. White, J. M., S. E. Delos, …, K. Schornberg. 2008. Structures and mechanisms of viral membrane fusion proteins: multiple variations on a common theme. *Crit. Rev. Biochem. Mol. Biol.* 43:189–219.
5. White, J. M. 1995. Membrane fusion: the influenza paradigm. *Cold Spring Harb. Symp. Quant. Biol.* 60:581–588.
6. Kielian, M., and F. A. Rey. 2006. Virus membrane-fusion proteins: more than one way to make a hairpin. *Nat. Rev. Microbiol.* 4:67–76.
7. Lai, A. L., Y. Li, and L. K. Tamm. 2005. Interplay of protein and lipids in virus entry by membrane fusion. *In* Protein-Lipid Interactions. L. K. Tamm, editor.. Wiley-VCH, pp. 279–303.
8. Epand, R. M. 2000. Membrane fusion. *Biosci. Rep.* 20:435–441.
9. Brecher, M., K. L. Schornberg, …, J. M. White. 2012. Cathepsin cleavage potentiates the Ebola virus glycoprotein to undergo a subsequent fusion-relevant conformational change. *J. Virol.* 86:364–372.
10. Ge, M., and J. H. Freed. 2009. Fusion peptide from influenza hemagglutinin increases membrane surface order: an electron-spin resonance study. *Biophys. J.* 96:4925–4934.
11. Lai, A. L., H. Park, …, L. K. Tamm. 2006. Fusion peptide of influenza hemagglutinin requires a fixed angle boomerang structure for activity. *J. Biol. Chem.* 281:5760–5770.
12. Lai, A. L., and L. K. Tamm. 2007. Locking the kink in the influenza hemagglutinin fusion domain structure. *J. Biol. Chem.* 282:23946–23956.
13. Lai, A. L., A. E. Moorthy, …, L. K. Tamm. 2012. Fusion activity of HIV gp41 fusion domain is related to its secondary structure and depth of membrane insertion in a cholesterol-dependent fashion. *J. Mol. Biol.* 418:3–15.
14. Budil, D. E., S. Lee, …, J. H. Freed. 1996. Nonlinear-least-squares analysis of slow-motion EPR spectra in one and two dimensions using a modified Levenberg-Marquardt algorithm. *J. Magn. Reson. A.* 120:155–189.
15. Liang, Z. C., and J. H. Freed. 1999. An assessment of the applicability of multifrequency ESR to study the complex dynamics of biomolecules. *J. Phys. Chem. B.* 103:6384–6396.
16. Ge, M., and J. H. Freed. 2003. Hydration, structure, and molecular interactions in the headgroup region of dioleoylphosphatidylcholine bilayers: an electron spin resonance study. *Biophys. J.* 85:4023–4040.
17. Ge, M. T., A. Costa-Filho, …, J. H. Freed. 2001. The structure of bleb membranes of RBL-2H3 cell is heterogenous: an ESR study. *Biophys. J.* 80:332a.
18. Smith, A. K., and J. H. Freed. 2009. Determination of tie-line fields for coexisting lipid phases: an ESR study. *J. Phys. Chem. B.* 113:3957–3971.

19. Ge, M., and J. H. Freed. 2011. Two conserved residues are important for inducing highly ordered membrane domains by the transmembrane domain of influenza hemagglutinin. *Biophys. J.* 100:90–97.

20. Dzikovski, B. G., P. P. Borbat, and J. H. Freed. 2004. Spin-labeled gramicidin a: channel formation and dissociation. *Biophys. J.* 87:3504–3517.

21. Dimitrov, A. S., S. S. Rawat, …, R. Blumenthal. 2003. Role of the fusion peptide and membrane-proximal domain in HIV-1 envelope glycoprotein-mediated membrane fusion. *Biochemistry.* 42:14150–14158.

22. Tamm, L. K., X. Han, …, A. L. Lai. 2002. Structure and function of membrane fusion peptides. *Biopolymers.* 66:249–260.

23. Li, Y., and L. K. Tamm. 2007. Structure and plasticity of the human immunodeficiency virus gp41 fusion domain in lipid micelles and bilayers. *Biophys. J.* 93:876–885.

24. Han, X., and L. K. Tamm. 2000. A host-guest system to study structure-function relationships of membrane fusion peptides. *Proc. Natl. Acad. Sci. USA.* 97:13097–13102.

25. Pereira, F. B., F. M. Goñi, …, J. L. Nieva. 1997. Permeabilization and fusion of uncharged lipid vesicles induced by the HIV-1 fusion peptide adopting an extended conformation: dose and sequence effects. *Biophys. J.* 73:1977–1986.

26. Kliger, Y., A. Aharoni, …, Y. Shai. 1997. Fusion peptides derived from the HIV type 1 glycoprotein 41 associate within phospholipid membranes and inhibit cell-cell fusion. Structure-function study. *J. Biol. Chem.* 272:13496–13505.

27. Brügger, B., B. Glass, …, H. G. Kräusslich. 2006. The HIV lipidome: a raft with an unusual composition. *Proc. Natl. Acad. Sci. USA.* 103:2641–2646.

28. Haque, M. E., and B. R. Lentz. 2002. Influence of gp41 fusion peptide on the kinetics of poly(ethylene glycol)-mediated model membrane fusion. *Biochemistry.* 41:10866–10876.

29. Jaroniec, C. P., J. D. Kaufman, …, A. Bax. 2005. Structure and dynamics of micelle-associated human immunodeficiency virus gp41 fusion domain. *Biochemistry.* 44:16167–16180.

30. Bodner, M. L., C. M. Gabrys, …, D. P. Weliky. 2004. Temperature dependence and resonance assignment of ^{13}C NMR spectra of selectively and uniformly labeled fusion peptides associated with membranes. *Magn. Reson. Chem.* 42:187–194.

31. Castano, S., and B. Desbat. 2005. Structure and orientation study of fusion peptide FP23 of gp41 from HIV-1 alone or inserted into various lipid membrane models (mono-, bi- and multibi-layers) by FT-IR spectroscopies and Brewster angle microscopy. *Biochim. Biophys. Acta.* 1715:81–95.

32. Marsh, D. 2007. Lateral pressure profile, spontaneous curvature frustration, and the incorporation and conformation of proteins in membranes. *Biophys. J.* 93:3884–3899.

33. Janmey, P. A., and P. K. J. Kinnunen. 2006. Biophysical properties of lipids and dynamic membranes. *Trends Cell Biol.* 16:538–546.

34. Han, X., J. H. Bushweller, …, L. K. Tamm. 2001. Membrane structure and fusion-triggering conformational change of the fusion domain from influenza hemagglutinin. *Nat. Struct. Biol.* 8:715–720.

35. Lorieau, J. L., J. M. Louis, and A. Bax. 2010. The complete influenza hemagglutinin fusion domain adopts a tight helical hairpin arrangement at the lipid:water interface. *Proc. Natl. Acad. Sci. USA.* 107:11341–11346.

36. Schmick, S. D., and D. P. Weliky. 2010. Major antiparallel and minor parallel β sheet populations detected in the membrane-associated human immunodeficiency virus fusion peptide. *Biochemistry.* 49:10623–10635.

37. Haque, M. E., V. Koppaka, …, B. R. Lentz. 2005. Properties and structures of the influenza and HIV fusion peptides on lipid membranes: implications for a role in fusion. *Biophys. J.* 89:3183–3194.

38. Tristram-Nagle, S., R. Chan, …, J. F. Nagle. 2010. HIV fusion peptide penetrates, disorders, and softens T-cell membrane mimics. *J. Mol. Biol.* 402:139–153.

39. Safran, S. A., T. L. Kuhl, and J. N. Israelachvili. 2001. Polymer-induced membrane contraction, phase separation, and fusion via Marangoni flow. *Biophys. J.* 81:659–666.

40. Israelachvili, J. N., and P. M. McGuiggan. 1988. Forces between surfaces in liquids. *Science.* 241:795–800.

41. Epand, R. M., and R. F. Epand. 2000. Modulation of membrane curvature by peptides. *Biopolymers.* 55:358–363.

42. Goñi, F. M., and A. Alonso. 1999. Structure and functional properties of diacylglycerols in membranes. *Prog. Lipid Res.* 38:1–48.

43. Zimmerberg, J., and L. V. Chernomordik. 1999. Membrane fusion. *Adv. Drug Deliv. Rev.* 38:197–205.

44. Haque, M. E., and B. R. Lentz. 2004. Roles of curvature and hydrophobic interstice energy in fusion: studies of lipid perturbant effects. *Biochemistry.* 43:3507–3517.

45. Liao, Z. H., L. M. Cimakasky, …, J. E. K. Hildreth. 2001. Lipid rafts and HIV pathogenesis: host membrane cholesterol is required for infection by HIV type 1. *AIDS Res. Hum. Retroviruses.* 17:1009–1019.

46. Miyauchi, K., Y. Kim, …, G. B. Melikyan. 2009. HIV enters cells via endocytosis and dynamin-dependent fusion with endosomes. *Cell.* 137:433–444.

47. Simons, K., and E. Ikonen. 1997. Functional rafts in cell membranes. *Nature.* 387:569–572.

48. Chang, D. K., S. F. Cheng, …, Y. T. Liu. 2008. Membrane interaction and structure of the transmembrane domain of influenza hemagglutinin and its fusion peptide complex. *BMC Biol.* 6:2.

49. Li, Z. N., B. J. Lee, …, D. A. Steinhauer. 2008. Length requirements for membrane fusion of influenza virus hemagglutinin peptide linkers to transmembrane or fusion peptide domains. *J. Virol.* 82:6337–6348.

50. Reuven, E. M., Y. Dadon, …, Y. Shai. 2012. HIV-1 gp41 transmembrane domain interacts with the fusion peptide: implication in lipid mixing and inhibition of virus-cell fusion. *Biochemistry.* 51:2867–2878.

51. Borbat, P. P., E. R. Georgieva, and J. H. Freed. 2013. Improved sensitivity for long-distance measurements in biomolecules: five-pulse double electron-electron resonance. *J. Phys. Chem. Lett.* 4:170–175.